Long Period Seismology on Europa: I. Physically Consistent Interior Models

F. Cammarano,[1] V. Lekic,[1] M. Manga,[1] M. Panning,[1] and B. Romanowicz[1]

Abstract.

In order to examine the potential of seismology to determine the interior structure and properties of Europa, it is essential to calculate seismic velocities and attenuation for the range of plausible interiors. We calculate a range of models for the physical structure of Europa, as constrained by the satellite's composition, mass, and moment of inertia. We assume a water-ice shell, a pyrolitic or a chondritic mantle, and a core composed of pure iron or iron plus 20 weight percent of sulfur. We consider two extreme mantle thermal states: hot and cold. Given a temperature and composition, we determine density, seismic velocities, and attenuation using thermodynamical models. While anelastic effects will be negligible in a cold mantle and the brittle part of the ice shell, strong dispersion and dissipation are expected in a hot convective mantle and the bulk of the ice shell. There is a strong relationship between different thermal structures and compositions. The "hot" mantle may maintain temperatures consistent with a liquid core made of iron plus light elements. For the "cold scenarios", the possibility of a solid iron core cannot be excluded and it may even be favored. The depths of the ocean and core-mantle boundary are determined with high precision, respectively 10 km and 40 km, once we assume a composition and thermal structure. Furthermore, the depth of the ocean is relatively insensitive (4 km) to the core composition used.

1. Introduction

Europa presents planetary scientists with a set of fascinating questions, not the least of which concerns the presence of a water ocean beneath its icy surface. Recent magnetometer data acquired by the Galileo flybys have confirmed the presence of an ocean beneath the ice layer (*Kivelson et al.*, 2000). Additionally, ice cracks observed in detailed images of the planet are consistent with flow of warm ice or water below the surface (*Greeley et al.*, 2000), and the near-infrared mapping spectrometer experiment probably detected hydrated salts on the surface (*Mc Cord et al.*, 2001). The ice-shell thickness on Europa is constrained in part by the morphology and modeling of impact craters. Based on impact melt-production models, observed craters require an ice shell at least 3 to 4 km thick (*Turtle and Pierazzo*, 2001). The relationship between depth and diameter of the craters suggests an ice-shell thickness of at least 19-25 km (*Schenk*, 2002). Nevertheless, any quantitative constraints on the ocean and ice-shell depths are difficult to obtain from existing observations (*Pappalardo et al.*, 1999; *Greenberg*, 2005).

Information about the interior physical conditions of a satellite is essential to understand its evolution and determine its likelihood of developing and sustaining a habitat for life. Recent studies have focused on modeling the evolution of the ice-shell by taking into account tidal effects in the ocean and the "warm" (viscous) part of the ice (*Sotin et al.*, 2002; *Tobie et al.*, 2003; *Moore*, 2006). However, it is not clear whether tidal heating plays an important role in Europa's mantle as it does for Io (e.g., *Ross and Schubert*, 1986). Recent computations of the tidal heating for a viscoelastic mantle layer and the related implications to the evolution of the planet (*Moore and Schubert*, 2000; *Hussmann and Spohn*, 2004) confirm the possibility of a hot, and possibly partially molten, mantle.

Measurements of the seismic response of Europa, remotely from an orbiter or using a lander, can greatly expand our knowledge of its internal structure. Despite this potential, the feasibility of a seismic experiment that would exploit natural sound sources (e.g., the opening of the cracks in the ice) to investigate the thickness of the ice shell and the ocean depth, has only recently been considered (*Kovach and Chyba*, 2001 and *Lee et al.*, 2003). Besides probing the ice shell, seismic data may provide information about the interior thermal and compositional structure of the satellite. In order to determine the potential of seismic signals to discriminate between different possible scenarios for the structure of Europa, it is essential to provide a family of reasonable physical models.

Existing models of the internal density structure of Europa which fit its mass and moment of inertia (e.g., *Anderson et al.*, 1998, *Kuskov and Kronrod*, 2001, 2005, *Sohl et al.*, 2002) indicate the presence of a denser silicate mantle and a metallic core below the superficial ice-water shell. Kuskov and Kronrod (2001, 2005) used thermodynamic modeling for both the water-ice shell and silicate mantle. They considered different chondritic compositions. They computed only bulk properties, however, and thermal profiles, not being relevant for their questions, were not addressed. In this work, we are interested in computing possible physical models (i.e., temperature and composition) which have a density structure that satisfies the mass and moment of inertia constraints, and also predict shear (and bulk) properties and the shear quality factor. In particular, we are interested in characterizing a range of models spanning extreme seismic radial structures within the range of possible temperatures and compositions for the interior of Europa. The aim of such models is to assess the potential of long-period seismology (frequencies of 0.001 to 0.1 Hz) to discriminate between different scenarios (see companion paper, *Panning et al.*, 2006). Owing to advances in thermodynamical modeling and improved knowledge of the shear properties of Earth's mantle minerals at high temperature and pressure from mineral

[1]Seismological Laboratory, University of California Berkeley, California, USA.

0148-0227/06/$9.00

physics, it is now possible to compute, in a self-consistent way, both bulk and shear properties for silicate compositions (e.g., *Stixrude and Lithgow-Bertelloni*, 2005). Furthermore, knowledge of shear-attenuation at seismic frequencies and high temperature is also constantly improving (e.g., *Jackson* 2000, *Faul and Jackson*, 2005). Fortunately, due to the relatively low pressures of Europa's interior, extrapolation to high pressure for both elastic and anelastic properties, which is a significant source of uncertainties for the Earth's mantle (e.g., *Cammarano et al.*, 2003), is less problematic for small planetary bodies.

Here we generate a set of physical models by assuming a three-layer composition: water-ice, silicate mantle (either pyrolitic or chondritic) and a metallic core (either solid iron or iron+sulfur), coupled with different thermal structures. Thermodynamic properties as a function of pressure and temperature are computed for each layer by using equations of state based on the most recent mineral physics data. The depth of the ocean and of the core-mantle boundary are constrained by the mass and moment of inertia for each physical model. We include temperature-dependent anelasticity effects, because these may serve to discriminate seismically between a hot, strongly attenuating mantle, and a cold one.

2. Composition

2.1. Water-ice layer

We use the IAPWS-95 pure water equation of state (*Wagner and Pruss*, 2002) which covers the pressure (P) and temperature (T) range of the possible Europa ocean. We implemented the equation of state (EOS) for ice given by Feistel and Wagner (2005), which is consistent with the water EOS. The shear modulus of ice is obtained by scaling the bulk modulus using a constant Poisson ratio of 0.226, which has been chosen in agreement with experimental measurements by *Gammon* (1983). Also, a recent EOS for salty water, but valid only in a limited range of P and T (*Feistel*, 2003), is implemented and compared with that for pure water. If other elements are mixed with pure water, e.g. ammonia, the melting temperature will be reduced, thereby rendering more likely the presence of a liquid water-rich ocean.

2.2. Silicate mantle layer

The presence of a silicate mantle under the water-ice layer is likely on Europa because of the presence of higher-than-average densities in the satellite interior - as obtained from fitting the moment of inertia - and by analogy with other planetary bodies. Each planetary body has a characteristic composition related to its unique creation and evolution. The composition of Europa's silicate mantle, therefore, remains unknown.

We consider a pyrolitic (Earth-like) mantle and a low-iron (between L and LL type) chondritic mantle, which is consistent with a large iron core (*Kuskov and Kronrod*, 2001). In terms of major oxide abundances, pyrolite is poor in iron and silica and richer in magnesium compared to a chondritic composition (table 1). This results in a different mineralogy (table 2), mainly characterized by a higher content in olivine ($\sim$ 56% vs 35% in mole percentage) and lower in pyroxenes ($\sim$ 30% vs 60%). Moreover, the composition of single phases will be different (table 2), e.g. olivine Mg# is 0.9 and 0.75 in the pyrolite and chondrite mantles, respectively. As a consequence, density is on average lower for pyrolite and seismic velocities are higher (table 2).

The presence of hydrous minerals would have the potential to strongly reduce the average mantle density, but, as pointed out by Anderson et al. (1998), at the relatively low pressures of the Europa mantle (<3 GPa), hydrated silicates break down and release their water at temperatures between 700°C and 800°C (*Ulmer and Trommsdorff*, 1995). Moreover, their presence will significantly decrease the solidus temperature, thereby favoring differentiation at relatively low temperatures. The likely presence of a metallic core and a deep ocean seem to indicate that such differentiation has probably occurred in Europa.

Thermodynamic properties of pyrolite at the pressure and temperature range of Europa are estimated by using a recent equation of state for a five oxide (CFMAS) system (*Stixrude and Lithgow-Bertelloni*, 2005) specifically constructed for shallow upper mantle conditions (i.e. P-T conditions that cover the entire Europan mantle) and including shear properties. Phase equilibria are determined by Gibbs free energy (G) minimization. The properties of pure species, including G, are specified for the isotropic part by a set of parameters (elasticity plus Helmholtz free energy and Debye temperature) which are given in Stixrude and Lithgow-Bertelloni (2005). The extrapolation at high pressure and temperature is done by using a Birch-Murnaghan EOS for the "cold" part and the quasi-harmonic Debye-Grüneisen approximation for the thermal part. A similar formulation has been constructed for the shear part and compiled parameters are also reported in Stixrude and Lithgow-Bertelloni (2005). The EOS has been implemented in an open-source thermodynamic modeling code (PERPLEX, www.perplex.ethz.ch by J. Connolly, e.g., *Connolly*, 2005), which solves the nonlinear free energy minimization problem by approximating the continuous compositional variations of solution phases with sets of discrete compositions and then using common linear minimization techniques.

The consistent determination of phase-equilibria diagrams and thermodynamic properties and the validity of the EOS for a large range of compositions permit its use for the L-LL chondritic type composition as well. The results for pyrolite - for example the density as a function of pressure (P) and temperature (T) (figure 1a) - are tested against an experimentally determined phase diagram and a different set of parameters (*Cammarano et al.*, 2003). Although not self-consistent, this approach allows us to vary the elastic parameters within boundaries estimated on mineral physics data and thus estimate uncertainties in seismic velocities and density at various P-T conditions for given compositions. Because of the good quality of the data at relatively low P and for a large T range, uncertainties in density (and seismic velocities) - for a given model - are very low, namely from $\sim$ 0.1% (0.2% for V_P, 0.4% for V_S) at low T to $\sim$ 0.3% (0.7% for V_P, 1.4% for V_S) at high T (*Cammarano et al.*, 2003). The chondritic densities are shown in figure 1b. The sharp changes in the phase diagram of both compositions, more pronounced in pyrolite, correspond to the plagiocase-spinel and spinel-garnet phase transitions. Note that maximum pressures at the bottom of Europa's mantle do not exceed 4 GPa.

The mineralogy of the chondritic composition (table 2) is slightly different from that inferred by other equations of state (e.g., *Kuskov and Kronrod*, 2001), particularly regarding the proportions at a given depth between OPX (higher in our case) and CPX (lower than Kuskov and Kronrod, 2001). However, these discrepancies only marginally affect the predicted density and seismic velocities.

2.3. The metallic core

The presence of a metallic core is hypothesized by analogy with other planetary bodies. Two compositions are tested: either pure iron, or iron and 20 weight percent sulfur, close to the eutectic proportions of the binary system. The presence of light elements considerably lowers density. Although other light elements may be present as well, sulfur surely is one of the best candidates, and the system Fe-FeS is well

known (e.g., *Sanloup et al.*, 2000; *Balog et al.*, 2003; *Waldner and Pelton*, 2005).

There exists trade-offs between the composition of the core, the thermal evolution and the present state of the planet. A pure iron core, which melts around 1900 K at pressures of Europa core, will be solid if the mantle is cold enough. Conversely, for the sulfur rich composition, the core is solid only if temperatures are below the melting eutectic temperature (around 1400 K at core pressure).

The phase diagram of pure iron at the relatively low pressures of Europa's core (not exceeding 5.5 GPa) is well known. We compiled data on elasticity and density for the stable phases: α phase (bcc-iron) at low T; γ phase (fcc-iron) at high T; and the liquid phase above melting temperature (table 3). Because the temperature will be nearly constant and the pressure gradient small, we prefer to estimate pressure and temperature derivatives already at the correct pressure and temperature and extrapolate linearly. The coefficients of thermal expansion, used to correct density at high temperature by

$$\rho\left(T,P_0\right)=\rho\left(T_0,P_0\right)e^{-\int_{T_0}^{T}\alpha(T')dT'} \quad (1)$$

are also compiled.

The eutectic melting temperature and its pressure dependence are also well known (e.g., *Boehler*, 1996). Data on density of the liquid and its change with sulfur content has also been measured at appropriate P-T conditions (*Sanloup et al.*, 2000). We do not include data on the elasticity of the solid phases which are stable below the eutectic temperature at Europa's pressures. However, we consider such low temperatures unlikely.

Data used and Clapeyron slopes between different iron phases are given in table 3.

3. Thermal structures

In this section, we define different thermal structures that may have evolved in Europa's interior in order to provide a benchmark for seismic measurements. We focus on extreme cases, either cold or hot, because they provide upper and lower bounds for seismic (elastic and anelastic) properties.

The interior thermal state of Europa is strongly related to its dynamics and evolution. Tidal heating can play an important role as it does on Io, and its magnitude depends on the assumed (unknown) rheology of the planet. Tidal heating may be pronounced in the warm ice, where it would regulate the thickness of the overlying layer in which heat conduction dominates (*Ojakangas and Stevenson*, 1989).

3.1. Ice-shell and ocean

After fixing the surface temperature T_0 at 110 K, compatible with average estimates based on Galileo data (*Spencer et al.*, 1999), we tune the temperature profiles to test a range of appropriate thicknesses for the ice shell (2 km to no ocean). The thermal profile in the top conductive part is calculated by using the solution of the general expression for the temperature in a spherical shell with internal heat production at steady-state (*Turcotte and Schubert*, 1982), i.e.:

$$T=T_0+\frac{\rho H}{6k}\left(a^2-r^2\right)+\left(\frac{\rho H r_b^3}{3k}-\frac{q_b r_b^2}{k}\right)\left(\frac{1}{a}-\frac{1}{r}\right) \quad (2)$$

where T_0 is the surface temperature, ρ is assumed constant here at 930 Kg/m^3; k= 2.6 W/mK is the thermal conductivity, also assumed constant. We neglect the temperature-dependence of thermal conductivity which decreases with increasing temperature from $\sim$ 4 W/m K, at surface, to 2.3 W/m K, at 260 K. a and r_b are respectively the radius at the top and at the bottom of the ice shell. H is the rate of heat production per unit mass (i.e. $H = Q_i/M$). The total heating Q is given by an internal tidal heating Q_i plus a basal heat flow q_b supplied to the base of the ice shell. Tidal heating depends on the thickness of the ice shell and its viscosity. Accurate thermal structures should include a self-consistent determination of the ice-shell thickness based on an assumed rheology (e.g., *Reese et al.*, 2005; *Moore*, 2006). For our purposes, we choose to not fully consider the coupling between rheological properties since our aim is to identify extreme cases. Moreover, we neglect the additional contribution of tidal dissipation within the convective part of the ice shell. As result, the computed thicknesses of the conductive lid are slightly over estimated.

For our thermal structures, we take a constant value of $Q_i = 2 \times 10^{12} W$, that is consistent with the values derived by the thermal equilibrium analysis of Moore (2006), which have a relatively narrow range between 0.6 to 2 $\times 10^{12}$ W. The thickness of the conductive lid is limited by a temperature that approaches the melting temperature - we assume a value of $0.95 \times T_{melt}$. The resulting conductive lid is $\sim$ 5 km for the 20 km thick ice shell and decreases when the ice shell thickens. Variations of -3 (+5) km in the thickness of the conductive top layer – which correspond to an order of magnitude increase (decrease) in internal heating Q_i – will affect only marginally the seismic response at low frequencies (see companion paper *Panning et al.*, 2006).

The basal heat flow q_b supplied to the ice shell is estimated in section 3.2 for a hot or cold mantle. We use those values for all the cases, except for the two extreme cases. For a given ice shell depth, and assuming the same internal heating, the conductive lid will be only 2 km thicker with the cold interior (q_b=5mW/m^2) than for the hot interior (q_b=40mW/m^2). This is due to the high constant value of the internal heating in Equation 2 compared to the additional basal heat.

For the 2 km thick ice-shell and for the one without an ocean below, q_b is computed to be consistent with those structures. In order to reach the melting temperature of ice at the bottom of the shell, the thinnest ice shell requires a hot interior with a very high heat flow. We computed q_b = 160 mW/m^2, that is four times more than the flux estimated for a hot mantle. The case of a pure ice shell without an ocean below would require an extremely cold interior, with a heat flow from the mantle not exceeding 3.0 mW/m^2, that is below the heat flow for our cold mantle case, later discussed. In addition, it requires a very low internal heating - three order of magnitude less than what is assumed - probably not consistent with realistic ice rheologies, even for relatively cold ice. We anticipate that this shell should have a depth around 130 km to satisfy mass and moment of inertia (see column for cold mantle case in table 5 and section 4.). Although unrealistic, we model this thermal structure because its seismic response is very different from that of the other cases (see *Panning et al.*, 2006).

Below the conductive lid, the temperature profile is assumed to be adiabatic. The adiabatic temperature profile is found by solving numerically the expression for its gradient:

$$\left(\frac{dT}{dz}\right)_S=\frac{\alpha T g}{C_P} \quad (3)$$

The heat capacity C_P and the thermal expansion α are computed with the corresponding equation of state. Because of the low pressure range, we do not introduce any high pressure correction for α (e.g, *Cammarano et al.*, 2003).

It is important to note that at equilibrium conditions, the thermal profile of the top, conductive part of the ice shell is independent of the regime of heat transport from below (conductive or convective).

We impose an increase in temperature of 15 K at the ice-water boundary, consistent with a convection model (*Nimmo and Manga*, 2002). We then have an isothermal temperature profile in the ocean.

3.2. Mantle and core

In building our mantle thermal structures, we would like to take into account the feedback between the amount of heat produced by radiogenic heat and the tidal heating. Two extreme thermal structures are possible: either radiogenic heat is not sufficient to augment the tidal heating, so that we have a cold, conductive mantle, or the radiogenic heating is high enough to stimulate further tidal heating.

To construct the extreme thermal structures, we use the same procedure used for the ice shell. We fix the parameters which enter in Equation 2 to typical average values (table 4), but, for one end-member, we consider a much smaller radiogenic heat (1.3×10^{11} W which results in a mantle heat flow of ~ 5 mW/m^2) with a negligible coupled tidal heating. For the high-temperature extreme, we consider a high tidal heating using a value of 8.5×10^{11} W, consistent with a hot, less viscous mantle, which is added to the normal radiogenic heat contribution, and results in a heat flow of $\sim$ 40 mW/m^2. If conditions that permit partial melting are reached at the base of lithosphere, enhanced tidal heating may even have the potential to produce volcanism. Note, however, that the viscosity for such extreme tidal heating should lower significantly and it would not be consistent, overall, with the eccentricity of Europa's orbit (e.g., *Hussmann and Spohn*, 2002).

The distribution of internal heating in the mantle and the possible contribution of heat from the core will dictate the mantle dynamics of the hot case. The extreme "hot" cases will be characterized by strong solid-state whole mantle convection. In the case of a purely internally heated convection, the adiabatic ($\sim$ isothermal) mantle is not required to have a thermal boundary layer at core-mantle transition.

We test two hot thermal structures (figure 2): the first lacking a thermal boundary layer and the second with an arbitrarily fixed ΔT of 400 K at the core-mantle discontinuity. This temperature jump has been chosen because it would increase the temperature at the core-mantle boundary, which is constrained by the melting temperature of the silicate ($\sim$1500 K), to the melting temperature of the pure iron ($\sim$1900 K). Note that we neglect the available heat coming from the core in constructing our simplified thermal structure for the mantle (i.e. we set $q_b = 0$ in the equation). Therefore, we do not have the expected bottom boundary layer for the second case, and the conductive lids for the two hot thermal structures are identical. Both hot thermal profiles are characterized by a relatively thin lithospheric mantle shell with an adiabatic thermal structure below.

It is noteworthy that all convective scenarios require that temperatures be close to the solidus throughout the mantle. As we shall see later, temperature-dependent anelasticity effects will produce markedly different seismic characteristics for the cold and hot cases, but different hot scenarios will have more similar (1-D) seismic structures.

In our opinion, the hot scenario seems more likely. Steady state thermal conduction curves obtained with uniform distribution of radiogenic elements and assuming average values of radiogenic heat production derived from silicate rocks ($\sim 2.1 \times 10^{11}$ W) would reach the melting temperature in the mid-mantle. Tidal heating effects will be enhanced at that depth, providing additional heat to the system. Moreover, if we assume a value of viscosity of 10^{21} Pa s, commonly adopted for Earth's shallow mantle, the Rayleigh number will be of order 10^5, greater than the critical value ($\sim 10^3$) to have convection. This consideration further supports the possible presence of a convective mantle, which implies, on average, an adiabatic thermal gradient far from the thermal boundaries.

Because the variation of pressure with depth is small, the adiabatic temperature profile in the core can be approximated by an isotherm (figure 2).

4. Inversion for ocean depth and core-mantle boundary depth

For any given combination of thermal structure and composition, we can calculate the depth of the ocean and of the core-mantle boundary which best fits the mass and moment of inertia of Europa (table 5). Given a physical structure, the uncertainties on those two depths, especially the ocean depth, are quite small and are mainly due to uncertainty in the moment of inertia of the satellite (figure 3). The small uncertainties in estimated density at the pressure range of the Europa mantle, quoted in section 2.2, have negligible effects on these results.

We choose not to invert for the gravity acceleration (g) profile, which requires tedious iteration because of the feedback with the density profile. Instead, we approximate the gravity profile by pre-computing the values at the core-mantle boundary (assuming an average density of the core, based on the composition used), at the ocean bottom (assuming an average density of the water-ice layer combined with information about Europa's total mass), taking the known values at the surface (~ 1.31 m/s^2) and at the center (0), and interpolating linearly between these points. The resulting gravity profile is sufficiently accurate, and does not noticeably affect our results.

For a given thermal structure, we find an increase in depth of ~ 50 km for the core-mantle boundary, but only ~ 15 km for the ocean depth when using the higher density chondritic mantle instead of pyrolite.

The cold and hot scenarios have trade-offs due to temperature effects on density (see figure 1). For a given composition, a cold mantle requires a deeper ocean and core-mantle boundary (see last two rows in table 5). Core composition is the dominant factor in determining the depth of the core-mantle boundary discontinuity, but has relatively little effect on the ocean depth (table 5). However the thermal state of the mantle, in spite of the trade-off with composition, still significantly affects this depth in the case of the lighter (thus shallower) core composition (table 5).

Variations in the thickness of the ice shell due to different imposed thermal structures in the shallower part of Europa do not significantly affect the depth of the ocean bottom and of the core-mantle boundary because of the small density contrast between water and ice. Specifically, when we increase the ice shell thickness from 2 to 80 km, we find that the depth of the ocean bottom decreases by $\sim$ 5km, while the depth of the core-mantle discontinuity increases by $\sim$ 2km.

In general, our estimates of the ocean depth are consistent with previous findings (*Anderson et al.*, 1998).

5. Anelasticity

Including anelastic effects is essential to accurately characterize the seismic response of the physical models. Viscoelastic relaxation at high temperatures leads to dispersion (frequency dependence of seismic wave speeds) and dissipation (attenuation). The development of experimental techniques to measure viscoelastic behavior at high temperatures and seismic frequencies (i.e. mHz-Hz) is beginning to provide direct constraints on the shear attenuation phenomena (e.g., *Faul and Jackson*, 2005). Anelasticity is strongly temperature-dependent and it can be used to discriminate

between the "cold" and the "hot" scenarios. Shear anelasticity (or quality factor) can be expressed as

$$Q_S = B\omega^{\gamma} exp\left(\frac{\gamma H(P)}{RT}\right) \quad (4)$$

with

$$H(P) = E + PV \quad (5)$$

where B is a normalization factor, ω is the seismic frequency, γ the exponent describing the frequency dependence of the attenuation, T the temperature, R the gas constant, E the activation energy, V the activation volume and H is the activation enthalpy. A useful homologous temperature scaling is (*Karato*, 1993):

$$g = \frac{H(P)}{RT_m(P)} \quad (6)$$

where the dimensionless factor g is a function of the activation enthalpy H, the melting temperature T_m and the gas constant R. Although it does not have a physical basis, the extrapolation of Q_S to high pressure using the melting temperature has been favored because it overcomes the lack of reliable data for the pressure dependence of the activation enthalpy. Extrapolation with pressure, which still present important challenges for the Earth, is less problematic for small planetary bodies where pressure does not increase dramatically with depth. In this sense, we expect a significant and constant attenuation throughout the "hot", adiabatic mantle. In the case of a cold mantle, we expect very weak attenuation in the mantle, possibly enhanced at the core-mantle boundary.

It must be noted that a grain-size sensitive attenuation, associated to a grain-boundary sliding mechanism, has been observed in laboratory experiments at seismic frequencies on Earth's mantle minerals (*Jackson et al.*, 2002). We decide to not model this mechanism, assuming, instead, that a similar grain size characterizes the hot and cold thermal structure. An increase in grain size, keeping all the other parameters fixed, will increase the quality factor (i.e., reduce attenuation) (*Cammarano et al.*, 2003). Although the trade-off between temperature and grain-size is not linear, an increase of 1 order of magnitude in size would approximately correspond to ∼100 K of temperature decrease in the mantle (*Faul and Jackson*, 2005).

In the mantle, we test anelastic effects using a model derived by *Cammarano et al.*, (2003) and used for the Earth's upper mantle. The model is consistent with experiments at seismic frequencies. The factor g (=30) and the weak frequency dependence γ (=0.2) are constrained by mineral physics experiments. The pre-exponential factor B=0.056 has been constrained by 1-D seismic attenuation profiles for the Earth. We take the peridotite solidus KLB1 (*Herzberg and Zhang,* 1996; *Hirschmann,* 2000) for both pyrolite and chondrite composition. The melting temperature of the two mantle compositions should be very similar (e.g., *Hirschmann et al.*, 2003) and certainly does not significantly affect the results. Bulk attenuation is assumed constant and very low throughout the mantle.

Temperature-dependent anelasticity can also be present in the convective ice-shell. We are not aware of any data at seismic frequencies for ice. Rheological data on pure ice (e.g.,*Durham and Stern*, 2001; *Goldsby and Kohlstedt*, 2001) suggest that a similar grain-size and temperature-dependent mechanism could be dominant. The thickness of the ice-shell is related to the grain size within. Based on equilibrium between the convective heat flow and the tidal heat generation, Moore (2006) computed - by using the Goldsby and Kohlstedt flow law - a grain size of 1 mm for a ice-shell of ∼ 16 km and one order of magnitude less for a ∼ 80 km thick shell. However, grain sizes found in deep ice-cores from the Earth's polar cap are much bigger (1 mm to 1 cm, *Montagnat and Duval, 2000*) - probably because of a grain boundary migration mechanism - and the dominant creep mechanism at low-stresses is also debated (e.g., see discussion *Goldsby and Koltstedt*, 2001, 2002 and *Duval and Montagnat*, 2002).

Because of the small increase of pressure and temperature within the convective ice-shell, grain size would have the dominant effect on the attenuation structure in the convective part of the ice shell, if the dominant deformation mechanism is grain-size sensitive. We decide to account for this effect by simply doubling the quality factor when we go from the thinnest to the thickest ice-shell, since the uncertainties in the grain size dependence of natural ice (i.e. with impurities) and direct constraints at seismic frequencies are still not available.

More difficult to assess is the absolute value for the seismic attenuation, i.e. extrapolate the viscosity law to the much smaller time scale typical of the seismic periods in which we are interested. Because of the high homologous temperature, the quality factor (Q_S) should be quite low (i.e., high seismic attenuation). We thus determine reasonable bounds for the values of the quality factors to be tested, since it is not possible to quantitatively estimate these values. The maximum value chosen is the quality factor measured for silicates at similar homologous temperatures (T/T_m). The non-dimensional factor g can be estimated to be ∼ 22 for the activation energy measured for the grain-boundary-sliding mechanism (49 kJ/mol). Assuming that the other parameters do not vary, this will lower the quality factor by a factor of 6 for the same homologous temperature. In this case, for a warm convective ice, we can reach quality factors as small as < 10. We expect these two extreme values to span the possible range of attenuation for ice. In addition, we take into account the effects of grain size dependence of attenuation by doubling the value when increasing the convective part of the ice shell from 0 to ∼ 100 km. Measurements of seismic attenuation at appropriate frequencies are required for better constraints.

Note that although similar activation laws, and possibly similar physical mechanisms, govern the rheological properties (i.e. viscosity), the time scale at which they operate is typically large enough to not affect the propagation of seismic waves at the low frequencies. The Maxwell relaxation time, which characterizes time-scales at which viscous behavior becomes important, can be, however, quite low for the warm part of the ice shell. If viscosity stays around values of 10^{14} Pa s, Maxwell time is on the order of $10^4 s$, but can be 10^2 s - similar to long period seismic waves - if viscosity is as low as 10^{12} Pa s.

While anelastic effects create what is usually called intrinsic seismic attenuation, scattering may further contribute to the attenuation of seismic waves. These effects will be particularly important in the shallow part of Europa's ice shell, where porosity could be high and a regolith layer may have formed, similar to the one that developed on the Earth's moon. Note, however, that the observed strong scattering effects on the moon should not be expected on Europa. Seismic observations for the moon found a very low intrinsic attenuation (high quality factor), but very high scattering effects, which give rise to the typical coda signal in the high frequency lunar signals (*Lognonne*, 2005) and are consistent with a cold interior and a surface regolith layer with large 3-D variations. On Europa the situation is different. The surface features indicate the presence of a flowing (and consequently more attenuating) ice not so far from the surface. The conductive top shell of the ice, as discussed before, will not be very thick and 3-D scattering effects will be less important than on the Earth's moon. More extensive discussion about the effects of a surface regolith layer and possible scattering effects due to 3-D structure are given in the companion paper (*Panning et al.*, 2006).

6. The 1-D physical models

Figures 4 and 5 show the seismic velocities, shear quality factor and density of the physical models for hot and cold scenarios. The largest difference between the various thermal scenarios is in the shear quality factors Q_S (seismic attenuation is $1/Q_S$) as shown in figure 4. In the hot cases, the effect of dissipation is to reduce the seismic velocities in the mantle, especially V_S. In the cold case, anelasticity does not play a significant role in modifying the expected seismic velocities (figure 5).

Thermal structures govern the main gradients in the velocity profiles. The hot case is characterized by a low velocity zone in the lithospheric mantle, where thermal effects prevail over pressure effects, and a positive constant gradient below, with a small increase corresponding to the spinel-garnet phase transition at $\sim$ 530 km (figure 5).

The properties of the hot and cold models are very different in the core (figure 5), because of the previously mentioned trade-off between core composition and thermal structure. In the eutectic core scenario, a shallower core-mantle boundary is accompanied by larger seismic velocities in the core, while the pure iron core is more compact and seismically faster. Although we believe that a core with light elements would be more consistent with the hot scenario, we also compute models with a pure iron core composition to be tested in our seismic simulations (table 5). The case of a cold, conductive mantle above a liquid eutectic iron-sulfur core is also computed (table 5).

Pyrolitic and chondritic mantles for both hot and cold case are considered in figure 6. The trade-off between temperature and composition in terms of seismic velocity and density is clear, but seismic attenuation is relatively insensitive to variations in dry composition.

7. Implications

Although we will undoubtedly wait many years or decades before having seismic data from Europa, some inferences on 3-D seismic structure may already be drawn. In the case of a hot scenario, the seismic structure of the Europa's interior will closely reflect temperature variations. In fact, the anelastic effects increase significantly the sensitivity of seismic velocities to temperature (e.g., as discussed in Cammarano et al., 2003), while compositional heterogeneity will have only secondary effects. Moreover, mantle flow may induce seismic anisotropy. Conversely, for a cold scenario, the thermal 3-D structure should be much more homogenous, and less sensitive to temperature, compared to the hot case. In the cold case, we expect a more uniform seismic structure and mantle anisotropy would be more difficult to form.

The cold and hot scenarios present substantial differences in terms of their seismic signature. In particular, hot mantle models are characterized by relatively strong dissipation and dispersion of the seismic signal. Seismic analysis of the models, eventually aimed at planning a seismic experiment that can provide the right information, is discussed in the companion paper (*Panning et al.*, 2006).

The trade off between the thermal state of the mantle and core composition lead us to favor two of the models among the ones tested (less likely models are identified by italics in table 5). A core rich in light elements is molten if the mantle is hot. Conversely, a solidified pure iron core is consistent with a cold conductive mantle.

Because of the different density of the two core compositions, the models will have a very different core-mantle boundary depths, as well as different seismic velocities. Also, the velocity profiles of the mantle will be different, although we do expect this to be challenging to distinguish, at least from the first seismic data from Europa.

In addition to the different seismic signature between the cold and hot thermal structures, the depths of possible natural seismic sources may be different as well. In the "hot" case, we may have a thin seismogenic region similar to the oceanic lithosphere on Earth. In the "cold" case, although more uncertain, it could still be possible to create enough stress due to tidal effects to generate deeper Europaquakes, similar to deep earthquakes observed on Earth's moon (see companion paper).

Finally, we point out that pressure- and temperature-dependent elastic and anelastic properties of complex materials plus the grid-search method to compute the depths of the main discontinuities for a given physical structure can be used, in principle, for any planetary body and provide a useful tool for characterizing the seismic response and plan a next generation of exploration missions.

8. Conclusions

We calculate a range of thermodynamically consistent models for the physical structure of Europa, as constrained by the satellite's mass and moment of inertia. We start with either a pyrolitic or a chondritic mantle composition and a core of either pure iron or iron plus 20% sulfur. The models completely characterize the radial seismic structure, i.e. elastic and anelastic properties, and they can be used to compute the seismic response of the planet.

The coupling between the thermal state of the ice shell and its viscosity dictates the ice-shell thickness and its seismic properties. It is likely that attenuation could be very high within the "warm", convective part of the ice shell.

Due to the feedback between radiogenic and tidal heating, two extreme thermal profiles are possible in the mantle. Strong dispersion and dissipation are expected in the hot convective mantle, while anelasticity effects will be much weaker in the case of the cold mantle.

There is a strong relationship between different thermal structures and compositions. The "hot" mantle may well keep temperatures high enough to be consistent with a liquid core made of iron plus light elements. In the case of the "cold scenarios", the possibility of a solid iron core cannot be excluded and it may even be favored.

The depth of the ocean and of the core-mantle boundary are determined with high precision once we assume a composition and thermal structure. Furthermore, the depth of the ocean is not very sensitive to the core composition used.

Acknowledgments. We thank Prof. Wolfgang Wagner for graciously providing us with the source code of the IAPWS-95 formulation for pure water. We thank Sebastien Merkel for help in selecting the iron elasticity data and Jamie Connolly for making his PERPLEX code available to the whole scientific community. Comments by Francis Nimmo, Antoine Mocquet and an anonymous reviewer significantly improved the manuscript. This work was supported in part by MIDAS, NASA grant No. NNG05GA25G.

References

Anderson W.W., Ahrens T., An equation of state for liquid iron and implications for the Earth's core. *J. Geophys. Res., 99,* 4273-4284, 1994

Anderson G.D., Schubert G., Jacobson R.A., Lau E.L., Moore W.B., Sjogren W.L., Europa's differentiated internal structure: inferences from four Galileo encounters, *Science, 281*, 2019-2022, 1998

Anderson O.L., Isaak D.G., Calculated curves for phase of iron. *American Mineralogist, 85,* 376-385, 2000

Balog PS, Secco RA, Rubie DC, Frost DJ., Equation of state of liquid Fe-10 wt% S: Implications for the metallic cores of planetary bodies. *J. Geophys. Res. 108,* art. n. 2124, 2003

Boehler R., Fe-Fe-S eutectic temperatures to 620 kbar. *Earth and Planetary Interiors 96,* 181-186, 1996

Cammarano F., Goes S., Giardini D., Vacher P., Inferring upper mantle temperatures from seismic velocities. *Phys. Earth Planet. Int., 138,* 197-222, 2003

Cassen P.M., Peale S.J., and Reynolds R.T., Structure and Thermal Evolution of the Galilean Satellites, in *Satellites of Jupiter,* D. Morrison, ed., University of Arizona Press, Tucson, Arizona, 93-128, 1982.

Connolly, J.A.D., Computation of phase equilibria by linear programming: A tool for geodynamic modeling and its application to subduction zone decarbonation. *Earth Planet. Sci. Lett., 236,* 524-541, 2005

Durham W.B., Stern L.A., Rheological properties of water ice - Applications to satellites of the outer planets *Annu. Rev. Earth Planet. Sci., 29,* , 295-330, 2001

Duval P., Montagnat M., Comments on "Superplastic deformation of ice: experimental observations", *J. Geophys. Res., 107,* doi:10.1029/2002JB000946, 2002

Faul U.H., Jackson I., The seismological signature of temperature and grain size variations in the upper mantle. *Earth Planet. Sci. Lett., 234,* 119-134, 2005

Feistel R., A new extended Gibbs thermodynamic potential of seawater. *Progress in Oceanography, 58,* 43-114, 2003

Feistel R., Wagner W., High-pressure thermodynamic Gibbs functions of ice and sea-ice. *J. Marine Res., 63,* 95-139, 2005

Gammon, P.H., Kiefte H., and Clouter M.J., Elastic Constants of Ice Samples by Brillouin Spectroscopy. *J. Phys. Chem., 87*, 4025-4029, 1983.

Goldsby D.L., Kohlstedt D.L., Superplastic deformation of ice: experimental observations *J. Geophys. Res.-Planets, 106,* 11017-11030, 2001

Goldsby D.L., Kohlstedt D.L., Reply to comments by P. Duval and M. Montagnat on "Superplastic deformation of ice: experimental observations", *J. Geophys. Res., 107,* doi:10.1029/2002JB001842, 2002

Goodman J.C., Collins G.C., Marshall J., Pierrehumbert R.T., Hydrothermal plume dynamics on Europa: Implications for chaos formation. *J. Geophys. Res.-Planets, 109,* art. E03008, 2004

Greeley R., Figueredo P.H., Williams D.A. et al., Geologic mapping of Europa. *J. Geophys. Res.-Planets, 105,* 22559 -22578, 2000

Greenberg R., Europa, the ocean moon, Springer-Praxis, 2005.

Herzberg C., Zhang J., Melting experiments on anhydrous peridotite KLB-1: Compositions of magmas in the upper mantle and transition zone. *J. Geophys. Res., 101,* 8271-8295, 1996.

Hirschmann M.M., Mantle solidus: experimental constraints and the effects of peridotite composition, *Geochem. Geophys. Geosyst. 1,* paper no. 2000GC000070, 2000

Hirschmann M.M., Kogiso T., Baker M.B., Stolper E.M., Alkalic magmas generated by partial melting of garnet pyroxenite. *Geology, 31,* 481-484, 2003

Hussmann H., Spohn T., Thermal-orbital evolution of Io and Europa. *Icarus, 171,* 391-410, 2004

Isaak D.G., Masuda K., Elastic and viscoelastic properties of α-iron at high temperatures. *J. Geophys. Res., 100,* 17689-17698, 1995

Jackson, I., Laboratory measurements of seismic waves dispersion and attenuation: recent progress, in "Earth's deep interior. Mineral physics and tomography from the atomic to the global scale" AGU, 265-289, 2000.

Jackson, I., J.D. Fitz Gerald, U.H. Faul, and B.H. Tan, Grain-size-sensitive seismic wave attenuation in polycrystalline olivine, *J. Geophys. Res., 107* (B12), 2360, doi:10.1029/2001JB001225, 2002.

Karato S., Importance of anelasticity in the interpretation of seismic tomography . *Geophys. Res. Letters, 20,* 1623-1626, 1993

Kivelson MG, Khurana KK, Russell CT, et al., Galileo magnetometer measurements: A stronger case for a subsurface ocean at Europa. *Science, 289,* 1340-1343, 2000

Klotz S., Braden M., Phonon dispersion of bcc iron to 10 GPa *Physic. Rev. Lett., 85,* 3209-3212, 2000

Kovach R.L., Chyba C.F., Seismic detectability of a subsurface ocean on Europa *Icarus, 150,* 279-287, 2001

Kuskov O.L., Kronrod V.A., Core sizes and internal structure of Earth's and Jupiters satellites.*Icarus, 151,* 204-227, 2001

Kuskov O.L., Kronrod V.A., Internal structure of Europa and Callisto *Icarus, 177,* 550-569, 2005

Lee SW, Zanolin M., Thode A., Pappalardo R.T., Makris N.C., Probing Europa's interior with natural sound sources. *Icarus,* 144-167, 2003

Lee S., Pappalardo R.T., Makris N.C., Mechanics of tidally driven fractures in Europa's ice shell. *Icarus,* 367-379, 2005

Lognonneé P., Planetary seismology. *Annu. Rev. Earth Planet. Sci., 33*, 571604, 2005

Mc Cord T.B., Orlando T.M., Teeter G., Hansen G.B., Sieger M.T., Petrik N.G., van Keulen L., Thermal and radiation stability of the hydrated salt minerals epsomite, mirabilite, and natron under Europa environmental conditions.*J. Geophys. Res., 106,* 3311-3319, 2001

Montagnat M., Duval P., Rate controlling processes in the creep of polar ice, influence of grain boundary migration associated with recrystallization. *Earth Planet. Sci. Lett., 183,* 179-186, 2000

Moore W.B., Schubert G., The tidal response of Europa. *Icarus, 147,* 317-319, 2000

Moore W.B., Thermal equilibrum in Europa's ice shell. *Icarus, 180,* 141-146, 2006

Nimmo F., Manga M., Causes, characteristics and consequences of convective diapirism on Europa. *Geophys. Res. Letters,29,* art. 2109, 2002

Ojakangas G.W., Stevenson D.J., Thermal state of an ice shell on Europa. *Icarus, 81,* 220-241, 1989

Panning M., Lekic V., Manga M., Cammarano F., Romanowicz B., Long period seismology on Europa: II. Predicted seismic response. *submitted to JGR-planets,* 2006

Pappalardo R.T., Belton M.J.S., Breneman H.H., Carr M.H., Chapman C.R. et al., Does Europa have a subsurface ocean? Evaluation of the geological evidence. *JGR-plantes, 104,* 24015-24055, 1999

Reese C.C., Solomatov V.S., Baumgardner J.R., Scaling laws for time-dependent stagnant lid convection ina spherical shell *Phys. Earth Planet. Int., 149,* 361-370, 2005

Ringwood A.E., Origin of the Earth and Moon. *Springer New York*, 1979

Ross M., Schubert G., Tidal dissipation in a viscoelastic planet. *J. Geophys. Res., 91,* 447-452, 1986

Sanloup C., Guyot F., Gillet P., Fiquet G., Mezouar M., Martinez I., Density measurements of liquid Fe-S alloys at high pressure. *Geophys. Res. Lett., 27,* 811-814, 2000

Schenk P.M., Thickness constraints on the icy shells of the galilean satellites from a comparison of crater shapes. *Nature, 417,* 419-421, 2002

Sohl F., Spohn T., Breuer D., Nagel K., Implications from Galileo observations on the interior structure and chemistry of the Galilean satellites. *Icarus, 157,* 104-119, 2002

Sotin C., Head III J.W., Tobie G., Europa: Tidal heating of upwelling thermal plumes and the origin of lenticulae and chaos melting. *Geophys. Res. Lett., 29,* 10.1029/2001GL013844, 2002

Spencer J.R., Tamppari L.K., Martin T.Z., Travis L.D., Temperatures on Europa from Galileo photopolarimeter radiometer: nighttime thermal anomalies. *Science, 284,* 1514-1516, 1999

Stixrude L., Lithgow-Bertelloni C., Mineralogy and elasticity of the oceanic upper mantle: Origin of the low-velocity zone. *J. Geophys. Res., 110,* B03204, doi:10.1029/2004JB002965, 2005

Turcotte D.L., Schubert G., Geodynamics. *Cambridge University Press,* 1982

Tobie G., Choblet G., Sotin C., Tidal heated convection: Constraints on Europa's ice shell thickness *J. Geophys. Res., 108,* 10.1029/2003JE002099, 2003

Turtle E.P., Pierazzo E., Thickness of a Europan ice shell from impact crater simulations *Science, 294,* 1326-1328, 2001

Turtle E.P., Pierazzo E., Thickness of a Europan ice shell from impact crater simulations *Science, 294,* 1326-1328, 2001

Ulmer P., Trommsdorff V., Serpentine stability to mantle depths and subduction-related magmatism. *Science, 268*, 858-861, 1995

Voronov F.F. and Chernysheva E.V., Anomalies in the elastic properties of silicious iron single crystals at pressures of up to 9 GPa and the alpha-epsilon phase transformation. *Phys. Solid State, 41,* 462-467, 1999

Wagner W., Pruss A., The IAPWS formulation 1995 for the thermodynamic properties of ordinary water substance for general and scientific purpose. *Journal of Physical and Chemical Reference Data, 31,* 387-535, 2002

Waldner P., Pelton A.D., Thermodynamic modeling of the Fe-S system. *Journal of Phase Equilibria and Diffusion, 26,* 23-38, 2005

F. Cammarano, Berkeley Seismological Laboratory, University of California Berkeley, 215 Mc Cone Hall, Berkeley, CA 94720, USA. (fabio@seismo.berkeley.edu)

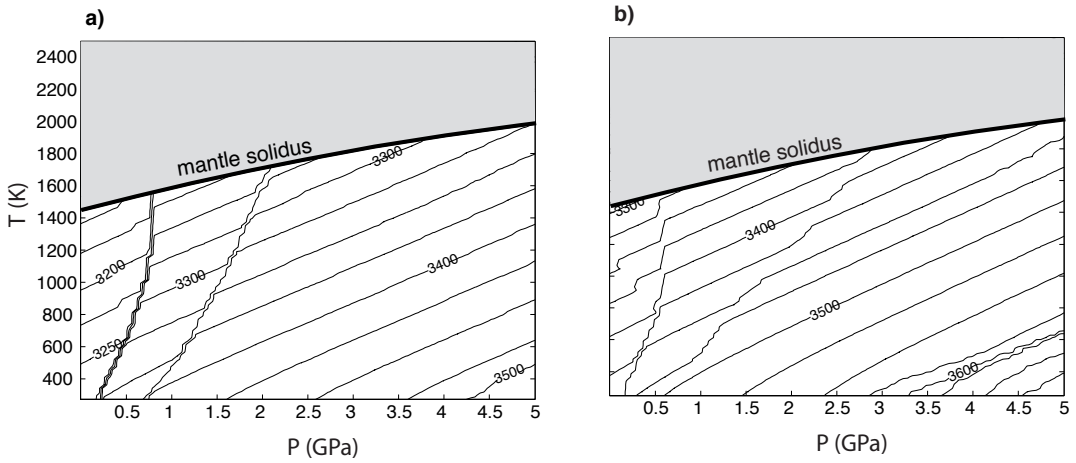

Figure 1. Density for pyrolite (a) and L-LL chondrite (b) composition as a function of pressure and temperature.

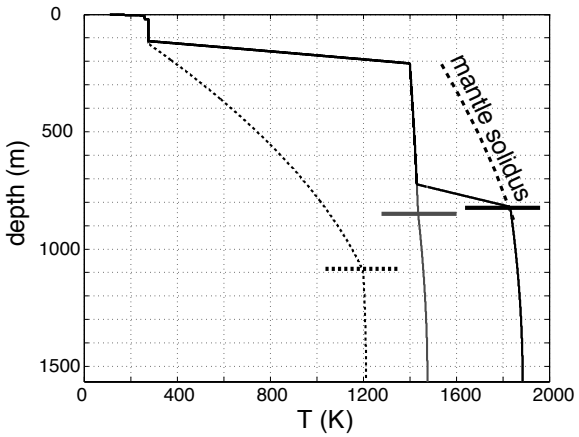

Figure 2. Thermal structures tested. Cold conductive structure is coupled with a pure solid iron. The two hot structures have here a Fe+20%S molten core.Horizontal lines indicate core-mantle boundaries for each structure. The profiles belong to the best-fit models for mass and moment of inertia.

Table 1. Bulk composition (in mol %)

	Pyrolite [a]	Chondrite (L-LL type) [b]
CaO	3.50	2.13
FeO	5.72	13.98
MgO	48.53	39.68
Al_2O_3	3.59	1.43
SiO_2	38.66	42.78

[a] from Ringwood (1979)

[b] mix of L and LL compositions as given in Kuskov and Kronrod (2001)

Table 2. Mineralogy (in mol %) and properties at 3 GPa and 1000 °C

	Pyrolite	Chondrite (L-LL type)	CaO[a]	FeO	SiO_2	MgO	Al_2O_3
Olivine	55.93	37.43	-	0.2-0.5	1.0-1.0	1.8-1.5	-
Garnet	13.38	3.58	0.12-0.12	0.42-0.90	3.02-3.02	2.48-2.00	0.98-0.98
OPX	15.34	49.74	-	0.52-1.12	3.96 -3.96	3.44-2.84	0.04-0.04
CPX	15.35	9.25	1.88-1.92	0.12-0.28	4.0-4.0	2.0-1.8	-
Density (kg/m^3)	3352.8	3456.2					
V_P (km/s)	8.09	7.61					
V_S (km/s)	4.57	4.32					

[a] first value for pyrolite, second for chondrite

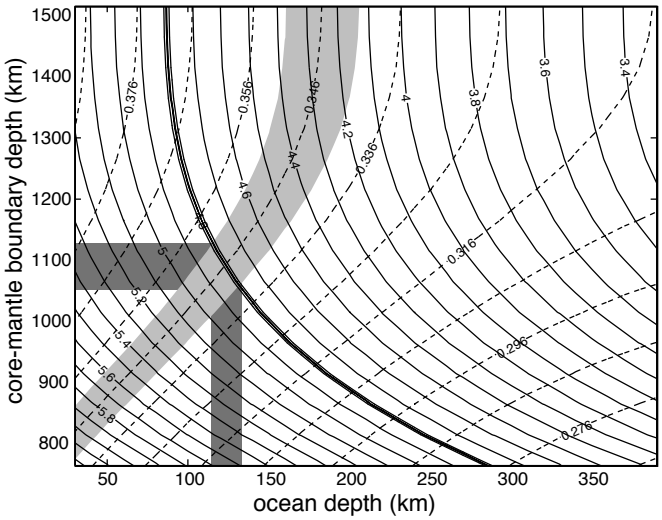

Figure 3. Ocean and core-mantle boundary depths for one physical structure - 20 km ice-shell, cold thermal structure, pyrolitic mantle and iron core composition. Solid lines contour mass (in 10^{22} Kg), dashed lines are for moment on inertia values. Uncertainties in the two discontinuity depths, denoted by dark gray boxes, are due to uncertainties in mass, equal to $4.800 \pm 0.015 \times 10^{22}$ kg (thick contour line), and uncertainties in moment of inertia (0.346 ± 0.005, *Anderson et al*, 1998), denoted by light gray.

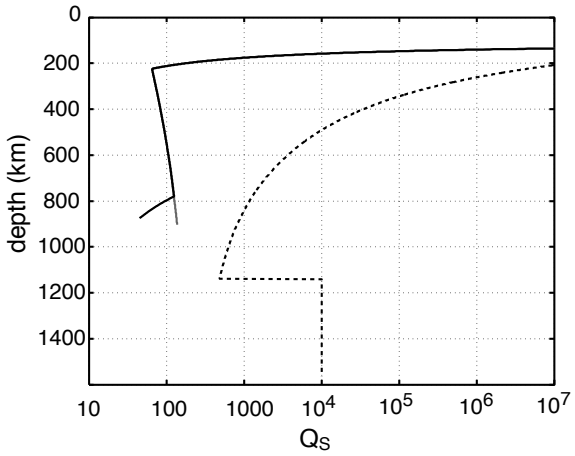

Figure 4. Shear Quality factor (Q_S) profiles of hot (solid lines, hot 1 in gray), vs cold scenarios (dashed lines).

Table 3. Iron and iron-sulfur properties

	bcc- α-iron	fcc- γ-iron	liquid	Fe-S (to max 20% S)
ρ (kg/m^3)	7873	8000	7000	5150-(% S-10)×50
α $(10^{-5}K^{-1})$	3.6	5	9.2	9.2
K_S (GPa)	167	156	109.7	53.2-(% S-10)×2
$\partial K_S/\partial P$	5.17	5.0	4.66	4.66
$\partial K_S/\partial T$ $(Pa\ K^{-1})$	-0.037	-0.040	-	-
G (GPa)	82	76.5	-	
$\partial G/\partial P$	2	2	-	
$\partial G/\partial T$ $(Pa\ K^{-1})$	-0.023	-0.023	-	
		Clapeyron slopes		
α/γ		T (K) = 1100 - 31.8 P (GPa)		
$\gamma/liquid$		T (K) = 1800 - 20.0 P (GPa)		
melting Fe-S eutectic		T (K) = 1280 + 13.0 P (GPa)		

[a] Density and thermal expansion of pure iron phases and the Clapeyron slopes between them are from *Anderson and Isaak*, 2000 and references therein. Elasticity at high pressure for α- and γ-iron from *Voronov and Chernysheva*, 1999, *Klotz and Braden*, 2000, thermal dependence from *Isaak and Masuda*, 1995. No data are compiled for shear pressure and temperature derivatives for γ-iron, properties for α phase have been used instead. Liquid iron properties from *Anderson and Ahrens*, 1994. All data for system FE-S are from *Sanloup et al.*, 2000 and references therein.

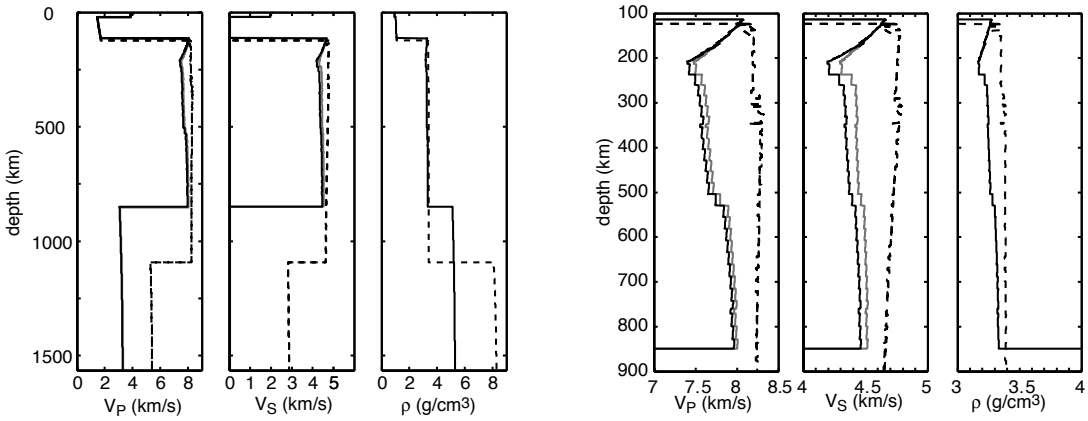

Figure 5. Physically consistent models for hot (solid lines) and cold (dashed) thermal structures with a pyrolitic mantle. Purely elastic models without dissipative effects are shown in light gray. The right panel shows a mantle close-up of the same models.

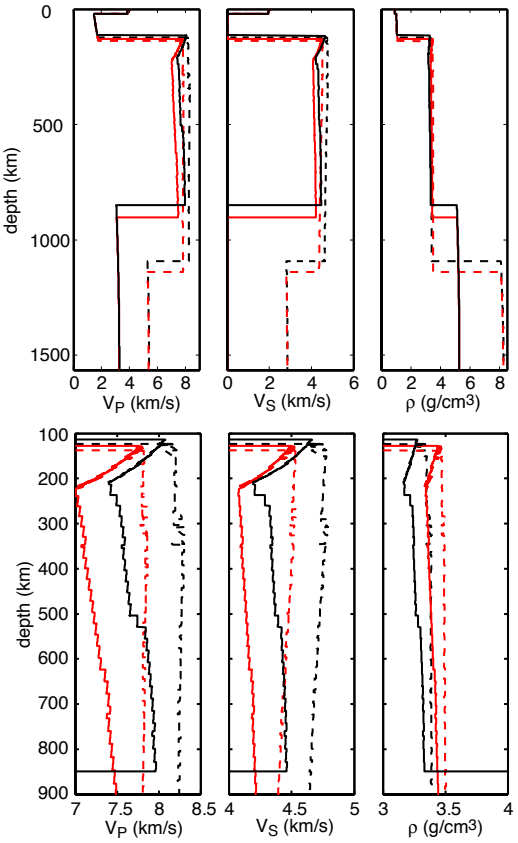

Figure 6. Physically consistent models for hot (solid lines) and cold (dashed) thermal structures for pyrolitic mantle (black) or chondritic (red). The right panel shows a mantle close-up of the same models.

Table 4. Average thermal parameters for the mantle

$T_0(K)$	273
$k(W/mK)$	4
$\rho(kg/m^3)$	3300
$a(km)$	1452 [b]
$r(km)$	730
$Q_R(10^{11}W)$[c]	2.1
$Q_H(10^{11}W)$	0.7 [d]

[a] Q_R= radiogenic heat for chondritic composition (*Hussmann and Spohn*, 2004 and reference therein). It corresponds to a mantle heat flow of 8 mW/m^2

[b] top (a) and bottom (r) of the mantle are kept fixed. Hence mass ($4/3\pi(a-r)$) as well. Note that the a variation of ± 100 km of r have negligible effects on the thermal profiles.

[c] H= $(Q_R + Q_H + Q_C)/m$, where heat from the core (Q_C) is set to 0

[d] tidal heating (Q_H) value for a solid body (*Cassen et al.*, 1982).

Table 5. Ocean and core-mantle boundary (CM) depths for different physical structures [a]

	Hot 1 [b]		Cold		Hot 2	
Mantle, Core composition	Ocean	CM	Ocean	CM	Ocean	CM
Pyrolite, Fe+20% S	113 ±11	849 ±51 [c]	*125 ±10*	*913 ±50*	114 ±11	820 ±54
Chondrite, Fe+20% S	128 ±10	902 ±62	*138 ±9*	*971 ±65*	128 ±10	874 ±65
Pyrolite, Fe	*109 ±10*	*1058 ±34*	123 ±9	1092 ±38	*109 ±10*	*1052 ±36*
Chondrite, Fe	*126 ±9*	*1100 ±42*	137 ±9	1140 ±48	*126 ±9*	*1094 ±42*

[a] Shallow thermal structure is fixed in all the models to have 20 km thick ice shell. All values in the table are in km

[b] Hot 1 model lacks a thermal boundary at core-mantle discontinuity, while hot 2 has ΔT =400 K.

[c] Uncertainties due to mass and moment of inertia uncertainties are given symmetric for sake of simplicity. In reality, there is a small discrepancy between maximum and minimum values, e.g., in this case the real values are 849+53 and 849-49 and 113+11.5 and 113-10.5 (see figure 1) Similar errors are in all the given uncertainties.

[d] Values in italics are given for the not likely pure iron core for the hot case and an eutectic iron-sulfur core for the cold case. The latter case has been inferred for a liquid core - eutectic temperature - instead than the extreme cold thermal structure in figure 2.